



Published in final edited form as:

Nat Genet. 2016 April ; 48(4): 349–355. doi:10.1038/ng.3511.

An expanded sequence context model broadly explains variability in polymorphism levels across the human genome

Varun Aggarwala¹ and Benjamin F. Voight^{2,3}

¹Genomics and Computational Biology Program, Perelman School of Medicine, University of Pennsylvania, Philadelphia, PA, USA

²Department of Systems Pharmacology and Translational Therapeutics, Perelman School of Medicine, University of Pennsylvania, PA, USA

³Department of Genetics, Perelman School of Medicine, University of Pennsylvania, PA, USA

Abstract

The rate of single nucleotide polymorphism varies substantially across the human genome and fundamentally influences evolution and incidence of genetic disease. Previous studies have only considered the immediate flanking nucleotides around a polymorphic site –the site’s trinucleotide sequence context– to study polymorph levels across the genome. Moreover, the impact of larger sequence contexts has not been fully clarified, even though context substantially influences rates of polymorphism. Using a new statistical framework and data from the 1000 Genomes Project, we demonstrate that a heptanucleotide context explains >81% of variability in substitution probabilities, revealing new mutation-promoting motifs at ApT dinucleotide, CAAT, and TACG sequences. Our approach also identifies previously undocumented variability in C-to-T substitutions at CpG sites, which is not immediately explained by differential methylation intensity. Using our model, we present informative substitution intolerance scores for genes and a new intolerance score for amino acids, and we demonstrate clinical use of the model in neuropsychiatric diseases.

INTRODUCTION

Measured at the level of the chromosome down to the individual base, rates of single nucleotide substitution vary substantially by position across mammalian genomes, including

Users may view, print, copy, and download text and data-mine the content in such documents, for the purposes of academic research, subject always to the full Conditions of use: http://www.nature.com/authors/editorial_policies/license.html#terms

Correspondence to: Benjamin F. Voight, PhD, Assistant Professor of Systems Pharmacology and Translational Therapeutics, Assistant Professor of Genetics, University of Pennsylvania, Perelman School of Medicine, 3400 Civic Center Boulevard, 10-126 Smilow Center for Translational Research, Philadelphia, PA 19104, ; Email: bvoight@upenn.edu

URLs:

Exome Variant Server (EVS), <http://evs.gs.washington.edu/EVS/>

AUTHOR CONTRIBUTIONS:

V.A. and B.F.V. conceived and designed the experiments, developed the model, performed the statistical analysis, developed and contributed analysis tools, and wrote the paper. B.F.V. supervised the research.

COMPETING FINANCIAL INTERESTS:

The authors declare no conflict of interest.

the humans¹. An exquisite example of the role for sequence context in contributing variability in substitution rate is provided by CpG dinucleotides, where spontaneous deamination of 5-methylcytosine results in ~14 fold higher C-to-T substitution rates compared to the genome-wide average^{1,2,3}. Modeling the variability in nucleotide substitution rates will inform our understanding of evolutionary processes, help identify functional noncoding regions⁴ and mutation promoting motifs, suggest mechanisms behind spontaneous mutation, and aid in prediction of the clinical impact of polymorphisms discovered through resequencing⁵. Such models will need to determine not only the optimal window of local sequence context but should also integrate knowledge of functional constraint on the genome due to pressure from purifying selection.

Studies of complex human disease have incorporated a simple trinucleotide sequence context^{6,7} into models to quantify the probability of *de novo* mutational events⁸⁻¹⁰, to clarify the distribution of somatic mutational events segregating in different cancers¹¹, and to model the purifying selective pressure on gene sequences¹². As their focus was clinical, these reports did not determine if this context model best captured the extent to which flanking nucleotides influence the variability in genome-wide nucleotide substitution rates. Here, we report a statistical framework that compares the extent to which different local sequence lengths influence the probability of nucleotide substitution, tested using data from the 1000 Genomes (1KG) Project¹³, apply our models to the coding genome, and demonstrate utility to interpret *de novo* mutations identified in studies of neuropsychiatric disorders. We define the probability of nucleotide substitution as the chance that a nucleotide in the human genome reference is polymorphic, that is, the nucleotide position segregates alternative nucleotides within the population. This probability depends upon population history, selection, sample ascertainment, and local context features that influence the rate of mutation.

RESULTS

Sequence context modeling of substitution probabilities

We hypothesized that local sequence context –the nucleotides that flank a polymorphic site– could explain the observed variability in nucleotide substitution probabilities. To test this hypothesis, we defined a statistical model (Supplementary Fig. 1, **Methods**) whereby the probability that a nucleotide substitution occurs at a genomic site varies according to (i) the identities of the nucleotides that flank the site and (ii) the size of the 5'-to-3' local sequence context window. To minimize the impact of natural selection, we focused on intergenic noncoding regions of the genome (**Methods**). As the estimated nucleotide substitution probabilities were robust (Supplementary Table 1a), we developed a likelihood-ratio testing procedure to evaluate competing local sequence context models (**Methods**).

First, we calculated the likelihood of the observed data assuming a “1-mer” model, which allowed different substitution classes (*e.g.*, A-to-G, C-to-T, etc.) to occur at different rates but ignored effects of sequence context on substitution probabilities. We compared the 1-mer model to the trinucleotide (“3-mer”) sequence context model where single 5' and 3' nucleotides flanking the polymorphic middle position impact the rate of substitution. As expected, the 3-mer model significantly improved fit to the data (log likelihood ratio, LLR =

6,070,948, $P \ll 10^{-100}$, Supplementary Table 1a). Next, we evaluated if additional local nucleotides could further improve fit to the observed data. We demonstrate that, when compared to the 3-mer model or the pentanucleotide ('5-mer') model (with two flanking nucleotides on each side), the larger, heptanucleotide ('7-mer') model (with three flanking nucleotides on each side) fit the data better (both LLR > 494,212, $P \ll 10^{-100}$, Supplementary Table 1b). To further validate the models, we estimated substitution probabilities using 1,659,929 HapMap¹⁴ variants found in our noncoding regions (**Methods**), and observed that 7-mer context probabilities strongly correlated with probabilities estimated from 1KG data (Supplementary Fig. 2, Supplementary Table 2), and provided the best fit to the observed polymorphisms (Supplementary Table 3). Our model recapitulates expected shifts in probabilities consistent with population histories¹⁵ (Supplementary Fig. 3) and the downward shift in the average substitution probability for the X chromosome¹⁶ relative to autosomes (Supplementary Table 4) due to the smaller effective population size at the X chromosome. Taken collectively, our analyses demonstrate for the first time, to our knowledge, that a 7-mer sequence context model explains the observed distribution of polymorphisms found in human populations.

To incorporate prior information, we developed a Bayesian formulation using objective conjugate priors for analysis of the noncoding genome (**Methods**). Consistent with our previous analysis, the 7-mer context model proved superior compared to all other models (Approximate Bayes Factor (ABF) $\gg 1,000$, Supplementary Table 1c). In subsequent analyses, we use these posteriors for the nucleotide substitutions probabilities.

7-mer context predicts noncoding substitution rates

To quantify the variance in the posterior probabilities that a 7-mer sequence context model could explain, we considered each substitution class separately, as well as CpG site contexts (nine classes total). We employed forward regression (**Methods**) to select features from a 7-mer context window to predict substitution probabilities and considered up to four-way interactions at positions within the window. When compared to single-base and position models without interactions, incorporating higher-order interactions substantially improved the fit to data (Supplementary Table 5). Specifically, we found that our selected models in a separately held test data set explained a median of 81% of the variability (as compared to 30% explained by the 3-mer context) in probabilities across all substitution classes, covering 84% of all mutational events and fitting well the probability of C-to-T substitution at CpGs (Table 1, Fig. 1A). Although we identified a common set of interactions across classes (Supplementary Table 6), many common features did not always influence substitution probabilities in the same way, and others had class-specific effects. These observations indicate that core and class-specific features based on sequence context are predictive of the potential for nucleotide substitution.

Methylation cannot fully explain patterns at CpG sites

The spontaneous deamination of 5-methylcytosine at CpG sites results in ~14-fold higher rates of C-to-T substitutions generally^{3,17}. Although a previous report indicated that divergence at CpG sites varies as a function of local context, the focus was on introns, and did not consider population-level polymorphisms in humans¹⁸. Thus, we hypothesized that

the surrounding sequence context further influences the probability of nucleotide substitution at CpGs, and examined the C-to-T substitution class within the subset contexts that contain CpG at position 4 and 5 in the 7-mer. Simulations using a model that ignored additional genomic context, or considered the 3-mer context (Supplementary Fig. 4), using a fixed CpG substitution probability generated significantly less variability in 7-mer CpG substitution probabilities than was empirically observed (empirical $P \ll 10^{-10}$, Fig. 1A). These data indicate that (i) not all CpG sites accrue substitutions at the same rate and (ii) that the sequence context surrounding CpG sites correlate with biological features or mechanisms that influence this rate.

To explore the possibility that the excess variability depends upon variation in methylation intensity across sequence contexts, we reanalyzed whole-genome bisulfite sequencing data obtained from germline and other tissues of healthy individuals^{19,20}. Comparing the CpG sites that are consistently methylated versus consistently unmethylated across subjects, we observed as expected that methylation correlates with an increase in the probability of C-to-T substitution ($P \ll 10^{-100}$, Supplementary Fig. 5). Unexpectedly, when we compared the methylation intensity in sperm at 7-mer CpG contexts with the probability of substitutions, we found a positive but imperfect correlation ($R^2 = 0.33$, $P < 10^{-90}$, Fig. 1B), with similar results in other tissues (Supplementary Fig. 6), noting instances of methylation status decoupled from substitution probabilities. For example, nearly every genomic instance of the sequence contexts GTACGCA and GATCGCA showed consistent methylation signals (both methylated in >94% of occurrences in sperm), the probability of C-to-T transition was more than two-fold different for these two contexts (0.148 vs. 0.07, respectively). These data are consistent with the hypothesis that local context features beyond DNA methylation influence probabilities of C-to-T transitions at CpG sites, though we cannot exclude the possibility that sub-tissue methylation differences could explain these patterns.

Identification of novel mutation-promoting motifs

We next investigated the substitution probabilities for 7-mer contexts partitioned by substitution class (Fig. 2, Supplementary Table 7). First, we noted that several classes, C-to-A, and C-to-G in addition to C-to-T, appeared to segregate as mixtures of two distributions, explainable by CpG effects. These observations are consistent with studies demonstrating elevated substitutions at CpGs in humans²¹, though this early work was not powered to measure context dependencies surrounding CpG sites as we are here. As the methylation transition state intermediate 5-formylcytosine can induce spontaneous C-to-A or C-to-G substitutions²², one possibility is that methylation also elevates these rates in this context. We next determined if local sequence context motifs –analogous to but beyond CpG dinucleotides– correlate with variable substitution probabilities across classes (**Methods**). We noted that poly-CG sequences in the lower tail of C-to-T substitutions for the CpG context were enriched ($P < 10^{-16}$, Table 2). This observation is consistent with previous reports²³ as this context is found proximal to genes (Supplementary Fig. 7) and is associated with lower methylation intensities (Supplementary Fig. 8). In the upper tail of the A-to-T substitution class, we observed a poly(T) + poly(A) motif in the outlier sequences ($P < 10^{-5}$, Table 2). We also observed a similar quad-A motif in the lower tail of the A-to-G class ($P < 10^{-10}$). One possible mechanism that may contribute is the ‘slippage’ of protein machinery

during DNA replication²⁴. Our analysis also revealed motifs without an obvious contributing mechanism. First, in the upper tail of CpG rates, we observed enrichment of a TACG motif ($P < 10^{-10}$, Table 2) that was strongly methylated (Supplementary Fig. 8), but curiously, a similar motif shifted by one position was enriched in the lower tail of the A-to-C class ($P < 10^{-4}$). Second, the ApT dinucleotide was found to elevate the substitution probabilities (Fig. 2) for the A-to-G ($P < 10^{-25}$) and A-to-T classes ($P < 10^{-17}$), though not statistically significantly so for A-to-C. Finally, we observed a CAAT motif also enriched in the upper tail of the A to G substitution class ($P < 10^{-53}$), reported in an earlier study of dbSNP variants²⁵. These latter cases indicate potentially new mechanisms contributing to elevated nucleotide substitutability, not documented by the commonly utilized trinucleotide context model. As a final robustness analysis, keeping in mind limitations due to variant ascertainment, we estimated the substitution probabilities using HapMap variants and found similar mutation promoting motifs across substitution classes (Supplementary Table 8).

Experiments to validate the noncoding rate model

If the estimated noncoding substitution probabilities reflect properties of mutation, one would expect that these rates should (a) not influenced by rates of recombination (b) strongly correlate with rates of species divergence²⁶, (c) be consistent for both rare and common genetic variants, and (d) also be reflected in *de novo* mutational events. We explored each of these predictions in turn. First, we estimated the 7-mer substitution rates from all intergenic noncoding variants separately for high and low recombination rate regions, and found a strong correlation between the two ($R^2 = 0.97$, $P \ll 10^{-100}$, Supplementary Fig. 9, **Methods**), indicating that substitution probabilities estimated from the noncoding genome are correlated across high and low rates of recombination. Next, using human-chimpanzee and human-macaque alignments over intergenic noncoding sequences, we found a strong correlation between divergence and substitution probabilities for our 7-mer contexts (both $R^2 = 0.96$, $P \ll 10^{-100}$, Supplementary Fig. 10, Supplementary Table 9, **Methods**). We then estimated 7-mer probabilities from all intergenic noncoding rare variants (singletons and doubletons) separately from low and high frequency variants (>1%), and found a strong correlation ($R^2 = 0.98$, $P \ll 10^{-100}$, Supplementary Fig. 11, **Methods**), as well as a superior 7-mer context fit to data across variant frequencies (Supplementary Table 10). Finally, we obtained 4,748 *de novo* mutational events from a high quality pedigree sequencing dataset on 78 parent-offspring trios²⁷. We tested for the presence of motifs we identified in Table 2 around *de novo* events, and observed a significant enrichment (Supplementary Table 11, **Methods**). Taken collectively, these findings provide additional validation for the hypothesis that our substitution probabilities capture features of germline mutation.

7-mer context also predicts exonic substitution rates

Assuming that the processes that generate spontaneous mutations apply uniformly across the genome, we hypothesized that sequence context could explain variability in substitution probabilities in the coding genome. We therefore extended our initial framework (Supplementary Fig. 1, **Methods**) to the coding genome by (i) using information obtained from our model on the noncoding genome as prior and (ii) allowing for context dependence of codons and local sequence context in our estimates of substitution probabilities to

accommodate purifying selective pressure²⁸. Our new model substantially improved the fit to the data compared to either 3-mer sequence context models with or without codon context (ABF \gg 1,000, Supplementary Table 12). To further validate, we tested our model on a different large scale exome-sequencing dataset from \sim 4,300 individuals²⁹, and noted that our 7-mer model fit patterns of exonic polymorphisms better than competing models (ABF \gg 1,000, Supplementary Table 12, **Methods**). These results demonstrate for the first time, that a broader sequence context –beyond simple codon or trinucleotide context– captures the forces that shape variability in nucleotide substitutions in the coding genome.

We then examined the posterior distribution of substitution probabilities for all contexts stratified by the type of amino acid substitution (Supplementary Fig. 12, Supplementary Table 13), and found excess variability in each class than expected under simulation (Supplementary Table 14, **Methods**). Next, we enumerated the substitution probability profiles for each amino acid change, and found certain nonsense and missense substitution probabilities to be higher than synonymous levels (Supplementary Fig. 13), partially explained by CpG contexts. These observations caution against the practice –invoked in rare-variant association tests– of ignoring codon and sequence context when testing for the burden of functional substitutions. Our results here demonstrate that functional substitutions may not be equally likely or tolerated with respect to purifying selection.

7-mer context improves power to detect pathogenic variants

We now turn to applications of our model to improve the interpretation of variation discovered by clinical re-sequencing. Efforts to prioritize variants from such studies often rely on classifying variants that are deleterious with respect to population genetic fitness, hypothesizing that such variants are more likely pathogenic³⁰. As our coding substitution probabilities are influenced both by forces of mutation (estimated from the noncoding genome) and selection, we hypothesized that the ratio of these probabilities quantifies the action of selective pressure, and could be used to prioritize pathogenic variants. To test this hypothesis, we calculated the log ratio of intergenic noncoding and coding substitution probabilities, defined as sequence constraint score, for missense (n = 48,450) and nonsense (n = 12,054) variants present in the Human Gene Mutation Database (HGMD, **Methods**)³¹. We observed that the distribution of sequence constraint scores for HGMD variants was shifted towards larger values (intolerance) compared to 1KG variants ($P \ll 10^{-100}$, Fig. 3A), compatible with the “intolerant variant, pathogenic variant” hypothesis. Moreover, the distribution of scores based on our 7-mer model was further shifted towards intolerance with a thicker tail, compared to a 3-mer model ($P \ll 10^{-100}$, Supplementary Fig. 14). These data demonstrate that a coding model that includes codon and a 7-mer context improves identification of variants that are potentially pathogenic.

Describing genic intolerance to mutation via 7-mer context

Several groups have argued that the power to identify causal disease genes from clinical resequencing data could be enhanced by incorporating estimates of selective constraint on genes^{12,32,33}. The underlying hypothesis behind this concept is that genes that are under selective constraint are more likely to have functional consequences and are therefore most likely to be pathogenic and have fewer functional variants (“intolerant gene, pathogenic

gene”). The community has successfully applied this concept to neurodevelopmental and psychiatric disorders³⁴, however the existing approaches have not incorporated the 7-mer sequence or codon context in their models.

Therefore, we applied our 7-mer coding substitution probabilities to develop an intolerance score (Supplementary Table 15, **Methods**) quantifying the difference between the expected and observed number of functional variants at a gene, with higher scores consistent with functional constraint. To further validate, we found gene scores on a separate, larger exome sequencing data set and observed a strong correlation between the two (Supplementary Fig. 15). We found that genes belonging to putatively essential or ubiquitously expressed categories, scored strongly for genic intolerance ($P \ll 10^{-100}$, Fig. 3B). In contrast, gene sets representing Keratin and Olfactory categories were found to be highly tolerant of functional changes (Fig. 3B). Next, we applied this to OMIM genes or known genes behind several neuropsychiatric disorders like Autism³⁵, Epilepsy³⁶, Developmental disorder³⁷ and Intellectual disability³⁸⁻⁴⁰, and found them to have significantly higher intolerance scores ($P \ll 10^{-100}$, Fig. 3B). We then compared our gene scores to previously reported scores (Supplementary Fig. 16, **Methods**), and found that our approach improved classification or performed comparably to other approaches³² for genes in each set, including the disease categories (Supplementary Table 16). These results demonstrate that the most accurate scoring of genic tolerance to functional substitution can be achieved by modeling 7-mer sequence and coding context.

An amino acid score for pathogenic variant prioritization

Beyond the average rate of amino acid replacement that a gene might tolerate, genes could be further intolerant to specific types of amino-acid substitutions, signifying added localized selective constraint or importance for gene functionality. Therefore, we developed a score measuring the intolerance at amino acid replacement level in a gene (Supplementary Table 17, **Methods**), after quantifying the difference between the expected and observed number of functional variants for a specific amino acid at a gene. Across all genes represented in HGMD with a large number of putatively pathogenic amino acid changes for a specific substitution, we found they segregate larger intolerance scores for that amino acid (empirical $P < 10^{-10}$). Moreover, a gene might score “tolerant” for functional substitution, but intolerant for specific amino acid changes. For example, Von Willebrand Factor (*VWF*), a blood glycoprotein involved in hemostasis, is tolerant to substitution overall (within top 8% of gene tolerance) but intolerant to cysteine substitution (within top 3.5% of cysteine intolerance). This data is consistent with a causal mechanism for von Willebrand disease; protein misfolding when cysteine residues are substituted⁴¹. We note that 5,652 genes segregate a profile similar to *VWF*: average genic tolerance, but amino acid intolerance.

Interpretation of *de novo* mutations discovered in Autism

Autism spectrum disorder is a disease with complex etiology, and recent efforts have aimed to identify *de novo* mutational events that may contribute to disease. To highlight the utility of gene^{12,32} and amino-acid scores, we applied them to interpret *de novo* mutations collected from 2,508 Autism spectrum disorder⁴² cases and 1,911 control family trios. First, we found that the most intolerant genes based on our gene score segregated a significant

burden of *de novo* mutations in cases as opposed to controls (OR = 1.66, $P < 0.0001$, Fig. 4A, **Methods**), even after removing known autism genes³⁵ (OR = 1.54, $P < 0.001$), and similar, though slightly attenuated burden using other scores (Fig. 4A). Next, we found that the average amino acid scores for *de novo* mutations at Autism genes in cases was higher (more intolerant) than that found in controls, or at other genes in cases ($P = 0.002$, Fig. 4B, **Methods**). We further observed higher (intolerant) average amino acid scores for variants in genes with a positive variant burden in cases, relative to controls (+2 or +3 allele count excess in cases, both $P < 0.01$, Fig. 4B). Finally, several genes from the excess allele count set stood out with amino-acid specific intolerance (all within top 4 percentile of intolerance): *MYO9B*, *WDFY3*, *NAV2*, *STIL*, and *SCUBE2*. Aside from *WDFY3*, these genes are generally ‘tolerant’, based on their gene-score, indicating utility of sub-gene wise measurement of functional intolerance. While *MYO9B* has been implicated in autism³⁵ and *WDFY3* deletions in a murine model has been shown to cause Autism like symptoms⁴³, our analysis points to the remaining candidates for future follow-up.

DISCUSSION

We report a sequence context model that explains patterns of nucleotide substitution observed in the human genome. Our motivation was based on the need to statistically evaluate competing models for sequence context. We demonstrate that the commonly used context that includes one nucleotide flanking a polymorphic site does not fully capture the complete spectrum of where, what type, and how frequently nucleotides are expected to change. Furthermore, by using population level data, rather than *de novo* or somatic events, we were able to improve the resolution of substitution models and identify novel mutation promoting motifs. Our approach also characterized average selective pressures operating in the coding genome at a finer level of detail. Our model indicates substantial variability across all amino acid replacement classes, and, in some cases, synonymous substitutions that were less prone to change than missense or even nonsense substitutions. We suggest that inference of the presence and strength of selection on genes might further benefit by incorporating information at this resolution.

One question in the field has been how much sequence context can explain patterns of nucleotide substitution in genomes⁴⁴. Our results suggest that a substantial fraction can be robustly predicted by sequence context alone, although specific substitution classes may require more than sequence context for their prediction. In evolutionary genetics studies, the set of substitutions that occur at nearly constant rates proportional to the lineage (i.e., most “clock-like”) is important for accurate dating divergence events⁴⁵. While we did not apply our model to other species, the strong correlation with divergence suggests our features are potentially conserved across primates.

We acknowledge that a number of features remain to be formally evaluated in the genome⁴⁶, for example, recombination in the coding genome⁴⁷ or replication timing⁴⁸. Our framework has the flexibility to model the complexity found in any sequences that contain features hypothesized to be important. We also acknowledge that context models beyond three flanking nucleotides were not considered. The regression approach we presented does

suggest that the 7-mer models could be refined, perhaps allowing broader context to be considered.

With an appropriate background model for nucleotide substitution, novel statistics for clinical re-sequencing studies can be envisioned, based on the occurrence of discovered variation. Such approaches may complement statistics that assay allele frequency differences between cases and controls at one or more polymorphic sites. Moreover, comparative genomics applications to identify non-neutrally evolving regions, genome alignments, or tree reconstruction⁴⁹, would benefit from accurate models of nucleotide substitution. While the underlying mechanisms that determine how nucleotide sequences change over time remain to be addressed, we posit that features identified from our model provide important clues in elucidating these fundamental principles.

ONLINE METHODS

Sourcing population samples

Samples were obtained from phase 1 of the IKG Project. We considered only the variants from African, European, and East Asian ancestries.

Selection of intergenic noncoding sequences

Intergenic sequences were defined as the full set of genomic sequences that are not annotated in ENSEMBL Biomart (version 75) and RefSeq Genes. We then removed centromeric, telomeric, repetitive regions and sequences not present in the accessibility mask (version 20120824) filter of the IKG project. Within these intergenic regions, we identified variants for the three populations for use in downstream analysis. More details in Supplementary Note.

Statistical framework to model substitution probabilities for intergenic noncoding regions

We initially describe a simple model that does not take into account local sequence context, and then build upon this by incorporating additional local sequence contexts.

Suppose that we observe n_C occurrences of nucleotide C in the reference genome. A subset of these n_C sites will be polymorphic within the population of individuals. Let n_{CA} represent the number of sites where a nucleotide change C-to-A has occurred. Similarly, n_{CG} is the number of sites where a change C-to-G has occurred and n_{CT} is the number of sites where a change C-to-T has occurred. Then the probability of nucleotide substitution or polymorphism within the population can be described using a multinomial distribution:

$$\frac{n_C!}{(n_C - n_{CA} - n_{CG} - n_{CT})! n_{CA}! n_{CG}! n_{CT}!} \alpha_{CA}^{n_{CA}} \alpha_{CG}^{n_{CG}} \alpha_{CT}^{n_{CT}} (1 - \alpha_{CA} - \alpha_{CG} - \alpha_{CT})^{(n_C - n_{CA} - n_{CG} - n_{CT})}$$

(1)

where the probabilities of observing a substitution from C-to-A, C-to-G, and C-to-T are expressed as a_{CA} , a_{CG} , and a_{CT} , respectively. After iterating over all possible substitutions (*i.e.*, A-to-C, A-to-G, A-to-T, C-to-A, C-to-G, C-to-T, T-to-A, T-to-G, T-to-C, G-to-A, G-to-C, G-to-T), we merged the reverse-complementary pairs (*e.g.*, A-to-C was merged with T-to-G, etc.) to yield 6 “substitution classes” as parameters for the simple model, which we refer to as the “1-mer” model. We then use maximum-likelihood estimation (MLE) to find the substitution probability estimates for all possible substitutions.

This model can be naturally extended to consider the effects of local sequence context by replacing the count of n_x occurrences of nucleotide X with the count of occurrences of a particular nucleotide sequence context. For example, if we want to consider the local sequence context ACA, then we count the number of times the 3-mer sequence ACA occurs (n_{ACA}) in the reference genome. A subset of n_{ACA} will be polymorphic at the middle position C within a given population. Thus, let $n_{ACA \rightarrow AAA}$ represent the number of sites where a nucleotide change C-to-A has occurred at the middle position, $n_{ACA \rightarrow AGA}$ for changes from C-to-G and $n_{ACA \rightarrow ATA}$ for changes from C-to-T at the middle position. After iterating over all possible nucleotides combinations at the two ends (4 possibilities at either side for a total of 16) and substitutions at the middle position (3 possible changes per nucleotides for a total of 12), we merged the reverse complementary pairs yielding 96 substitution classes as parameters for the “3-mer” model.

Analogously, we extended the size of the sequence context window to evaluate the “5-mer” model and the “7-mer” model by considering additional fixed nucleotides (2 and 3, respectively) on either side of the polymorphic site, thereby estimating a total of 1,536 parameters for the 5-mer model and 24,576 parameters for the 7-mer model. More details in Supplementary Note.

Log-likelihood ratio testing for model comparison

We initially find the likelihood of the observed distribution of polymorphic sites using the substitution rate parameters for a sequence context model. We then calculate the likelihood ratio test statistic as:

$$-2\ln(L[data|context S_1]) + 2\ln(L[data|context S_2]) \quad (2)$$

where S_1 and S_2 represent parameters estimated from two competing sequence context models. The test is chi-squared distributed, with degrees of freedom equal to the difference in the number of parameters between the two models (*e.g.*, comparing the 3-mer model versus the 1-mer model requires 90 degrees of freedom; comparing the 7-mer model versus the 3-mer model requires 24,480 degrees of freedom).

Selection of HapMap variants

Single nucleotide polymorphic variants were obtained from phase 3 release of the HapMap project. We considered only the variants from African ancestry present in our intergenic noncoding sequences. More details in Supplementary Note.

Incorporating prior information into the statistical framework

Since the likelihood of our framework is based on a multinomial distribution, we utilize its conjugate prior, *i.e.*, the dirichlet distribution, for different sequence context models. For inference in the intergenic, noncoding genome, we selected the objective version of the prior for our analysis, with all concentration parameters of the dirichlet prior as 1. We then use MAP to find the substitution probability estimates for all possible substitutions. More details in Supplementary Note.

Bayes Factor analysis for model comparison

We calculated the approximate posterior likelihood, using the Chib's method, on the overall data using the maximum *a posteriori* (MAP) estimates of the substitution probabilities for a specific sequence context model found before. We then calculate the approximate Bayes factor as:

$$\frac{\text{Posterior likelihood under Model}_2}{\text{Posterior likelihood under Model}_1} = \frac{\text{Prob}(\text{Data}|\text{Context } S_2) \times \text{Prob}(\text{Context } S_2)}{\text{Prob}(\text{Data}|\text{Context } S_1) \times \text{Prob}(\text{Context } S_1)} \quad (3)$$

where S_1 and S_2 represent parameters estimate from two competing sequence context models. We use the Jefferey's scale for interpreting the approximate Bayes Factors, where the ratio if greater than 100 is considered to be decisive evidence against the Model₁. More details in Supplementary Note.

Regression modeling and feature selection

We considered each substitution class separately and created an additional substitution class for each of the three possible changes within a CpG context, resulting in nine substitution classes. For each substitution class, we considered the initial regression model:

$$Pr[X_1 \rightarrow X_2|S] = \alpha + \beta_1 p_1^C + \beta_2 p_1^G + \beta_3 p_1^T + \dots + \beta_n p_7^T + \varepsilon \quad (4)$$

where the probability that a nucleotide changes from X_1 to X_2 is modeled using a position-base variable p , a set of bases (*e.g.*, {C, G, or T} where A is the reference base) denoted by the superscript for p , each position (= 1, 2, 3, 5, 6, or 7) denoted by the subscript for p within sequence context S , intercept α , and error term ε . We assigned A as the reference nucleotide at each position and encoded the single nucleotide present at each position as the combination of three thermometer variables (*e.g.*, 0,0,0 = A; 0,0,1 = C; 0,1,0 = G; 1,0,0 = T). Next, we examined non-additivity (*i.e.*, interactions) between nucleotides at sequence context positions. Rather than including all possible interaction terms, we employed feature selection (*i.e.*, model training and testing to select the most informative features) and incorporated these terms into the final model. We considered 2-way, 3-way, and 4-way interactions across positions within the 7-mer as:

$$\begin{aligned}
 &Pr[X_1 \rightarrow X_2|S] \\
 &= \alpha + \beta_1 p_1^C + \beta_2 p_1^G + \beta_3 p_1^T + \dots + \beta_n p_7^T + \beta_a p_i^w \times p_j^x + \dots + \beta_b p_i^w \times p_j^x \times p_k^y + \dots + \beta_c p_i^w \times p_j^x \times p_k^y \times p_l^z + \dots + \varepsilon
 \end{aligned}
 \tag{5}$$

where the probability that a nucleotide changes from X_1 to X_2 is modeled as described in Equation 4, and a set of additional terms related to interactions is also incorporated. The effect of the interaction is represented by terms β_a for 2-way interactions, β_b for 3-way interactions, and β_c for 4-way interactions. We then divided the genome into two distinct sets for feature selection, using all even-numbered chromosomes for training and all odd-numbered chromosomes for model testing. During training, we performed stepwise forward regression for each level of interaction in order of increasing complexity (*i.e.*, first 2-way, then 3-way, and finally 4-way). For each level of interaction, we further trained the model by sequentially incorporating interaction terms, one at a time, and evaluating whether each term improved the model using the ANOVA F-test. The most informative interaction term was added to the model at each step. For higher-order (3-way and 4-way) interactions, we ensured that a proposed feature maintained the hierarchy constraint (*i.e.*, a selected 4-way term must bring with it all of its associated 3-way and 2-way terms), thereby adding degrees of freedom to our F-test assessment. We repeated this process until no additional features further improved the model (*i.e.*, all proposed features were $P > 0.001$ by the F-test). As our final model, we selected the trained model with the lowest mean-squared error, calculated via cross-validation within each substitution class. The 3-mer calculations considered all 2-way interactions plus single (*i.e.*, position 3 and 5 only) features. More details in Supplementary Note.

Sourcing CpG methylation data

We obtained CpG methylation data for our intergenic regions of interest from whole genome bisulphite sequencing studies performed on germline¹⁹ (sperm, oocyte), blastocyst, blood and brain²⁰ tissues. We performed our analysis on the 7,059,740 intergenic CpG sites that were methylated and the 651,479 intergenic CpG sites that were unmethylated in all 3 samples in the sperm tissue. We summarized the methylation signal across all samples for a tissue by calculating the mean intensity.

Sequence motif Identification

We examined the top and bottom 10 sequences for each substitution class, and manually identified a total of 6 motifs that we tested in each substitution class, stratified by CpG context. This results in a total of (9 substitution classes) * (2 tails, high and low) * (6 motifs) = 108 total tests. Note that we required a nominal $P = 4.6 \times 10^{-4}$ (Bonferroni correction for multiple testing). Testing was performed via Fisher's exact test. More details in Supplementary Note.

Recombination and substitution rates

We obtained recombination rate map of the YRI population from the phase 1 release of the 1KG project, and segregated our intergenic noncoding regions of interest into high (rate >3 cM/Mb) and low recombination rate (rate < 0.05 cM/Mb) regions. More details in Supplementary Note.

Human and primate divergence

We obtained human-chimpanzee and human-macaque chain and netted alignments from the golden path directories in the UCSC genome browser and found divergence between the human-primate pair by calculating fixed differences between the aligned intergenic noncoding sequences at each 7-mer sequence context. More details in Supplementary Note.

Variants across the frequency spectrum

We defined the rare variants as those occurring fewer than two times in the population, and low or high frequency variants as those with MAF >1%. We only considered the intergenic noncoding variants present in 1KG project belonging to the African ancestry, and found 2,789,383 rare and 8,019,893 low/high frequency variants. More details in Supplementary Note.

De novo mutations

We only considered the *de novo* mutations occurring in the accessible regions of the 1KG project. For each motif class, we found the expected number of mutations under a normalized 1-mer sequence context model. More details in Supplementary Note.

Extension of the substitution probability framework in the coding region

To model substitution probabilities for the coding genome, we utilized the statistical model developed for intergenic regions with the following modifications: First, we accounted for codon position-effects (*i.e.*, a given sequence context around a polymorphic site may occur at three different positions on a codon), which can lead to amino acid changes that may be subject to different levels of selective constraint. Second, we utilized probabilities learned from the intergenic noncoding region model as our Bayesian prior for the coding model. The parameters for this dirichlet distribution prior include the weighted baseline probabilities from the intergenic noncoding region as shape parameters. More details in Supplementary Note.

Selection of coding sequences

We selected exonic coordinates of the longest transcript for each gene annotated in ENSEMBL Biomart (version 75). We only considered those transcripts where (i) total exonic region length was a multiple of 3 and (ii) 90% or larger of it was present in the combined accessibility mask (version 20120824) filter of the 1KG project. This yielded 16,386 autosomal transcripts and 679 transcripts from the X chromosome.

To test our model in a different data set, SNP sites for ~4300 individuals of European ancestry were obtained from the Exome Variant Server (EVS, downloaded on August 26th

2013). For EVS data, to obtain a representative spectrum of allele frequencies (and impact of background selection) observed from the smaller set of individuals found in the 1KG data, we only considered variants with frequency greater than 0.03%. More details in Supplementary Note.

Annotation of SNP variants in the autosomal coding genome

For both 1KG and EVS data, we manually annotated the type of codon change caused by each variant specific to the transcript.

Scaling the substitution probability estimates for a larger sample

To calibrate our model (built using the 1KG dataset) for use with the larger EVS dataset, we rescaled the substitution probabilities estimated using 1KG data to make them proportional to the EVS dataset. We used a constant scaling factor defined as:

$$\frac{\text{Over all Substitution probability in the new dataset}}{\text{Over all Substitution probability in the 1KG dataset}} \quad (7)$$

on all substitution probabilities in the new dataset.

Simulating variability in substitution probabilities within amino acid replacement classes

We start by randomly distributing the observed substitutions within the amino acid replacement class, using a fixed rate model. We then calculate the respective 7-mer probabilities from the randomized data set using our multinomial distribution model for randomization, and then find the variance in the new substitution probability estimates for that class. We use 10^6 simulations to generate the distribution of substitution probabilities.

Measuring the effects of selection on polymorphisms in the coding region

To minimize the effects of selection on initial estimates of substitution probabilities, we selected intergenic noncoding intervals for model development. Assuming that the mechanisms that introduce new mutations into coding regions are similar to those at work in the noncoding genome, we inferred that the relative ratio of coding-to-noncoding substitution probabilities could indicate natural selection occurring in the coding genome. To quantify the effect of selection on substitution probabilities, we measured the \log_{10} ratio of coding-to-noncoding substitution probabilities using all coding variants observed in the 1KG African group. More details in Supplementary Note.

Calculating tolerance scores for genes

We find the expected distribution of polymorphism levels for each gene by performing simulations from the standard multinomial distribution using our coding substitution probability estimates. We then normalize the difference between the observed levels of polymorphism and those generated from simulations, to obtain gene tolerance score defined as:

$$\frac{(\mu_{NS} - n_{NS})}{\sigma_{NS}} \quad (8)$$

where μ_{NS} and σ_{NS} represent the mean and standard deviation of nonsynonymous polymorphisms generated from simulations based on our model, and n_{NS} is the empirical number of nonsynonymous polymorphism observed in the data. A positive gene score indicates that the number of observed substitutions is fewer than expected, and identifies genes experiencing stronger than average purifying selection.

Categorizing genes based on tolerance scores

We subdivided genes into various categories – *i.e.*, essential genes (where the mouse homolog knock-out is lethal), ubiquitously expressed genes, genes with known phenotypes described in OMIM, immune-related genes, keratin genes, and olfactory genes. The dataset from³³ was used to find the first two categories, while³² was used to classify OMIM genes. OMIM sub-categorizes genes according to mutational models, including *de novo*, dominant, haploinsufficient, or recessive. In our analysis, we merged OMIM's *de novo*, dominant, and haploinsufficient categories, treating them as a single category. We used the DAVID ontology database (version 6.7) to classify immune-related, keratin, and olfactory genes. We considered the gene list published in the latest *de novo* sequencing analysis papers of Autism³⁵, Epilepsy³⁶, Intellectual disability³⁸⁻⁴⁰ and Developmental disorder³⁷, as the gene set belonging to these diseases. We merged the gene lists of the aforementioned diseases, treating them as single category belonging to “All Neuropsychiatric disease”.

AUC comparison between competing gene scores on different gene sets

We used the receiver operating characteristic (ROC) curve to compare the performance of our gene scores against previously annotated scores for classifying genes into the gene sets we described above. We fitted a linear classifier using the three different gene scores, on each gene set and found the area under the curve (AUC) for each. More details in Supplementary Note.

Calculating tolerance scores for amino acids

We find the expected distribution of polymorphism levels for a specific amino acid within a gene by performing simulations from the standard multinomial distribution using our coding substitution probability estimates. Within a given gene, we then normalized the difference between the observed numbers of changes at a specific amino acid versus the number of changes expected from simulation using the equation:

$$\frac{(\mu_{AA} - n_{AA})}{\sigma_{AA}} \quad (9)$$

where μ_{AA} and σ_{AA} represent the mean and standard deviation of the specific amino acid replacement polymorphisms generated from simulations based on our model, and n_{AA} is the empirical number of amino acid replacement polymorphisms observed in the data. We

consider the normalized value in Equation 9 as the final tolerance score for that amino acid within the given gene. We interpret a positive amino acid (AA) tolerance score to indicate that the observed number of changes for that specific amino acid within the given gene was *even fewer* than expected. Thus, the AA tolerance score serves to identify amino acids experiencing stronger than average purifying selection.

Sourcing information about pathogenic variants

We used the Human Gene Mutation Database (HGMD professional 2014.4) to identify pathogenic variants for our autosomal genes of interest, which supplied 60,504 variants distributed over 3,647 genes for 5,359 putative human disorders.

Application of gene and amino acid score on Autism spectrum *de novo* sequencing data

We used the *de novo* sequencing data for Autism spectrum disorder⁴², to test the efficacy of our gene and amino acid score approach in identifying and prioritizing novel genes and variants associated with Autism. We found the *de novo* mutations belonging to cases and controls separately for each of our genic sequences of interest and considered a total of 2,171 mutations in 2,508 cases and 1,421 mutations in 1,911 controls. For a uniform comparison of gene scores across different approaches^{12,32}, we only considered the top 752 intolerant genes identified from each approach. We choose 752 genes because this was the number of intolerant genes identified in¹², which mapped to our autosomal genic sequences of interest (i.e., which pass the stringent criteria of sequencing quality in the 1KG project). We used the Odds ratio to find the burden of *de novo* mutations in cases as opposed to controls, in the set of intolerant genes. Fisher's exact test was used to compare the significance of burden. For amino acid score, all statistical comparisons were performed using the Wilcoxon sum ranked test. More details in Supplementary Note.

Code Availability

The computational pipelines used for probability estimation for the noncoding and coding genomes, and for forward regression and feature selection are available on request.

Supplementary Material

Refer to Web version on PubMed Central for supplementary material.

Acknowledgments

The authors would like to thank Casey Brown, Maja Bucan, Paul Babb, Katie Siewert, Kelsey Johnson, Stacie Bumgarner, and two anonymous reviewers for helpful comments on the manuscript. B.F.V. is grateful for support of the work from the Alfred P. Sloan Foundation (BR2012-087), the American Heart Association (13SDG14330006), the W.W. Smith Charitable Trust (H1201) and the NIH/NIDDK (R01DK101478).

References

1. Hodgkinson A, Eyre-Walker A. Variation in the mutation rate across mammalian genomes. *Nat Rev Genet.* 2011; 12:756–66. [PubMed: 21969038]
2. Ehrlich M, Wang RY. 5-Methylcytosine in eukaryotic DNA. *Science.* 1981; 212:1350–7. [PubMed: 6262918]

3. Rideout WM, Coetzee GA, Olumi AF, Jones PA. 5-Methylcytosine as an endogenous mutagen in the human LDL receptor and p53 genes. *Science*. 1990; 249:1288–90. [PubMed: 1697983]
4. Arbiza L, et al. Genome-wide inference of natural selection on human transcription factor binding sites. *Nat Genet*. 2013; 45:723–9. [PubMed: 23749186]
5. Yang Y, et al. Clinical whole-exome sequencing for the diagnosis of mendelian disorders. *N Engl J Med*. 2013; 369:1502–11. [PubMed: 24088041]
6. Hwang DG, Green P. Bayesian Markov chain Monte Carlo sequence analysis reveals varying neutral substitution patterns in mammalian evolution. *Proc Natl Acad Sci U S A*. 2004; 101:13994–4001. [PubMed: 15292512]
7. Blake RD, Hess ST, Nicholson-Tuell J. The influence of nearest neighbors on the rate and pattern of spontaneous point mutations. *J Mol Evol*. 1992; 34:189–200. [PubMed: 1588594]
8. Neale BM, et al. Patterns and rates of exonic de novo mutations in autism spectrum disorders. *Nature*. 2012; 485:242–5. [PubMed: 22495311]
9. Michaelson JJ, et al. Whole-genome sequencing in autism identifies hot spots for de novo germline mutation. *Cell*. 2012; 151:1431–42. [PubMed: 23260136]
10. Fromer M, et al. De novo mutations in schizophrenia implicate synaptic networks. *Nature*. 2014; 506:179–84. [PubMed: 24463507]
11. Lawrence MS, et al. Mutational heterogeneity in cancer and the search for new cancer-associated genes. *Nature*. 2013; 499:214–8. [PubMed: 23770567]
12. Samocha KE, et al. A framework for the interpretation of de novo mutation in human disease. *Nat Genet*. 2014; 46:944–950. [PubMed: 25086666]
13. Abecasis GR, et al. An integrated map of genetic variation from 1,092 human genomes. *Nature*. 2012; 491:56–65. [PubMed: 23128226]
14. The International HapMap Consortium. A haplotype map of the human genome. *Nature*. 2005; 437:1299–320. [PubMed: 16255080]
15. Campbell MC, Tishkoff SA. African genetic diversity: implications for human demographic history, modern human origins, and complex disease mapping. *Annu Rev Genomics Hum Genet*. 2008; 9:403–33. [PubMed: 18593304]
16. Schaffner SF. The X chromosome in population genetics. *Nat Rev Genet*. 2004; 5:43–51. [PubMed: 14708015]
17. Nachman MW, Crowell SL. Estimate of the Mutation Rate per Nucleotide in Humans. *Genetics*. 2000; 156:297–304. [PubMed: 10978293]
18. Mugal CF, Ellegren H. Substitution rate variation at human CpG sites correlates with non-CpG divergence, methylation level and GC content. *Genome Biol*. 2011; 12:R58. [PubMed: 21696599]
19. Okae H, et al. Genome-wide analysis of DNA methylation dynamics during early human development. *PLoS Genet*. 2014; 10:e1004868. [PubMed: 25501653]
20. Hovestadt V, et al. Decoding the regulatory landscape of medulloblastoma using DNA methylation sequencing. *Nature*. 2014; 510:537–41. [PubMed: 24847876]
21. Walser JC, Furano AV. The mutational spectrum of non-CpG DNA varies with CpG content. *Genome Res*. 2010; 20:875–82. [PubMed: 20498119]
22. Kamiya H, et al. Mutagenicity of 5-formylcytosine, an oxidation product of 5-methylcytosine, in DNA in mammalian cells. *J Biochem*. 2002; 132:551–5. [PubMed: 12359069]
23. Deaton AM, Bird A. CpG islands and the regulation of transcription. *Genes Dev*. 2011; 25:1010–22. [PubMed: 21576262]
24. Levinson G, Gutman GA. Slipped-strand mispairing: a major mechanism for DNA sequence evolution. *Mol Biol Evol*. 1987; 4:203–21. [PubMed: 3328815]
25. Panchin AY, Mitrofanov SI, Alexeevski AV, Spirin SA, Panchin YV. New words in human mutagenesis. *BMC Bioinformatics*. 2011; 12:268. [PubMed: 21718472]
26. Lanfear R, Welch JJ, Bromham L. Watching the clock: studying variation in rates of molecular evolution between species. *Trends Ecol Evol*. 2010; 25:495–503. [PubMed: 20655615]
27. Kong A, et al. Rate of de novo mutations and the importance of father's age to disease risk. *Nature*. 2012; 488:471–5. [PubMed: 22914163]

28. Bustamante CD, et al. Natural selection on protein-coding genes in the human genome. *Nature*. 2005; 437:1153–7. [PubMed: 16237444]
29. Fu W, et al. Analysis of 6,515 exomes reveals the recent origin of most human protein-coding variants. *Nature*. 2013; 493:216–20. [PubMed: 23201682]
30. Cooper GM, Shendure J. Needles in stacks of needles: finding disease-causal variants in a wealth of genomic data. *Nat Rev Genet*. 2011; 12:628–40. [PubMed: 21850043]
31. Stenson PD, et al. The Human Gene Mutation Database: building a comprehensive mutation repository for clinical and molecular genetics, diagnostic testing and personalized genomic medicine. *Hum Genet*. 2014; 133:1–9. [PubMed: 24077912]
32. Petrovski S, Wang Q, Heinzen EL, Allen AS, Goldstein DB. Genic intolerance to functional variation and the interpretation of personal genomes. *PLoS Genet*. 2013; 9:e1003709. [PubMed: 23990802]
33. Georgi B, Voight BF, Bu an M. From mouse to human: evolutionary genomics analysis of human orthologs of essential genes. *PLoS Genet*. 2013; 9:e1003484. [PubMed: 23675308]
34. Uddin M, et al. Brain-expressed exons under purifying selection are enriched for de novo mutations in autism spectrum disorder. *Nat Genet*. 2014; 46:742–7. [PubMed: 24859339]
35. De Rubeis S, et al. Synaptic, transcriptional and chromatin genes disrupted in autism. *Nature*. 2014; 515:209–215. [PubMed: 25363760]
36. Allen AS, et al. De novo mutations in epileptic encephalopathies. *Nature*. 2013; 501:217–21. [PubMed: 23934111]
37. Large-scale discovery of novel genetic causes of developmental disorders. *Nature*. 2015; 519:223–8. [PubMed: 25533962]
38. Hamdan FF, et al. De Novo Mutations in Moderate or Severe Intellectual Disability. *PLoS Genet*. 2014; 10:e1004772. [PubMed: 25356899]
39. Rauch A, et al. Range of genetic mutations associated with severe non-syndromic sporadic intellectual disability: an exome sequencing study. *Lancet*. 2012; 380:1674–82. [PubMed: 23020937]
40. De Ligt J, et al. Diagnostic Exome Sequencing in Persons with Severe Intellectual Disability. *N Engl J Med*. 2012; 367:1921–1929. [PubMed: 23033978]
41. Ginsburg D, Bowie EJ. Molecular genetics of von Willebrand disease. *Blood*. 1992; 79:2507–19. [PubMed: 1586703]
42. Iossifov I, et al. The contribution of de novo coding mutations to autism spectrum disorder. *Nature*. 2014; 515:216–221. [PubMed: 25363768]
43. Orosco LA, et al. Loss of Wdfy3 in mice alters cerebral cortical neurogenesis reflecting aspects of the autism pathology. *Nat Commun*. 2014; 5:4692. [PubMed: 25198012]
44. Eyre-Walker A, Eyre-Walker YC. How much of the variation in the mutation rate along the human genome can be explained? *G3 (Bethesda)*. 2014; 4:1667–70. [PubMed: 24996580]
45. Kimura M, Ohta T. On some principles governing molecular evolution. *Proc Natl Acad Sci U S A*. 1974; 71:2848–52. [PubMed: 4527913]
46. Séguirel L, Wyman MJ, Przeworski M. Determinants of mutation rate variation in the human germline. *Annu Rev Genomics Hum Genet*. 2014; 15:47–70. [PubMed: 25000986]
47. Hussin JG, et al. Recombination affects accumulation of damaging and disease-associated mutations in human populations. *Nat Genet*. 2015; 47:400–404. [PubMed: 25685891]
48. Koren A, et al. Genetic Variation in Human DNA Replication Timing. *Cell*. 2014; 159:1015–1026. [PubMed: 25416942]
49. Siepel A, Haussler D. Phylogenetic estimation of context-dependent substitution rates by maximum likelihood. *Mol Biol Evol*. 2004; 21:468–88. [PubMed: 14660683]

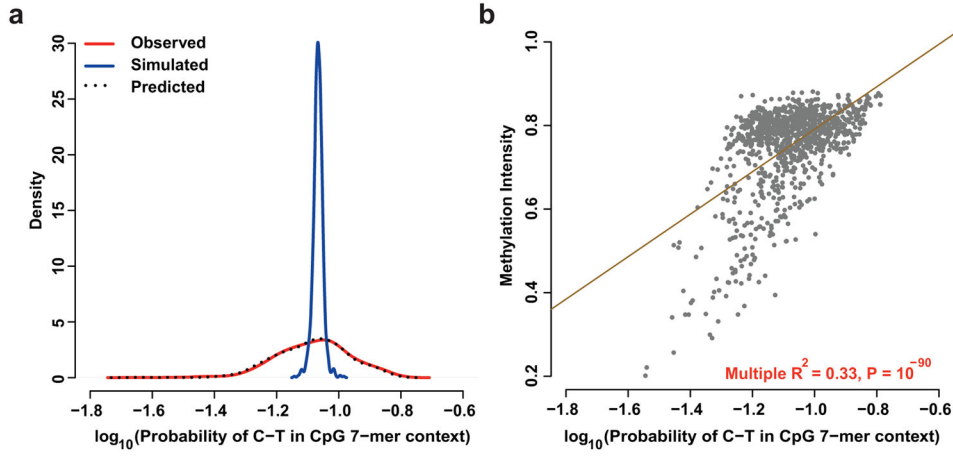


Figure 1. C-to-T substitution probabilities and methylation patterns within 7-mer CpG sequence contexts. **(a)** Simulations based on a fixed C-to-T substitution rate (blue) at CpG contexts do not capture the observed distribution of substitution probabilities (red) within the 7-mer sequence context. Rates predicted from our regression model (black) closely match the substitution probabilities observed under the 7-mer sequence context ($R^2 = 0.93$). **(b)** Correlation between average methylation intensity versus probability of C-to-T substitution in CpG 7-mer context.

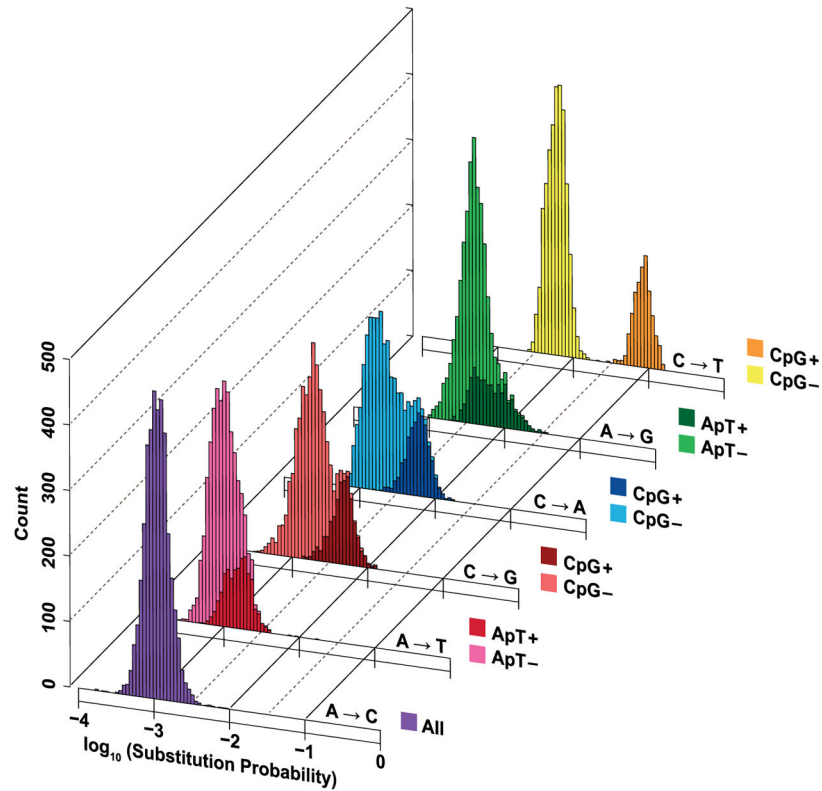


Figure 2.

Posterior probabilities of all classes of nucleotide substitution in the intergenic noncoding genome, estimated using the 7-mer context model. Sequences contexts are further stratified by color to indicate either the presence of a CpG (C at the polymorphic 4th position and G at the 5th position, for C-to-A, C-to-G and C-to-T substitution classes = CpG+; else CpG-) or the ApT state (A at the polymorphic 4th position and T at the 5th position, for A-to-G and A-to-T substitution classes = ApT+; else ApT-). For A-to-C, the ApT state did not significantly contribute to variability in the estimated probability distribution.

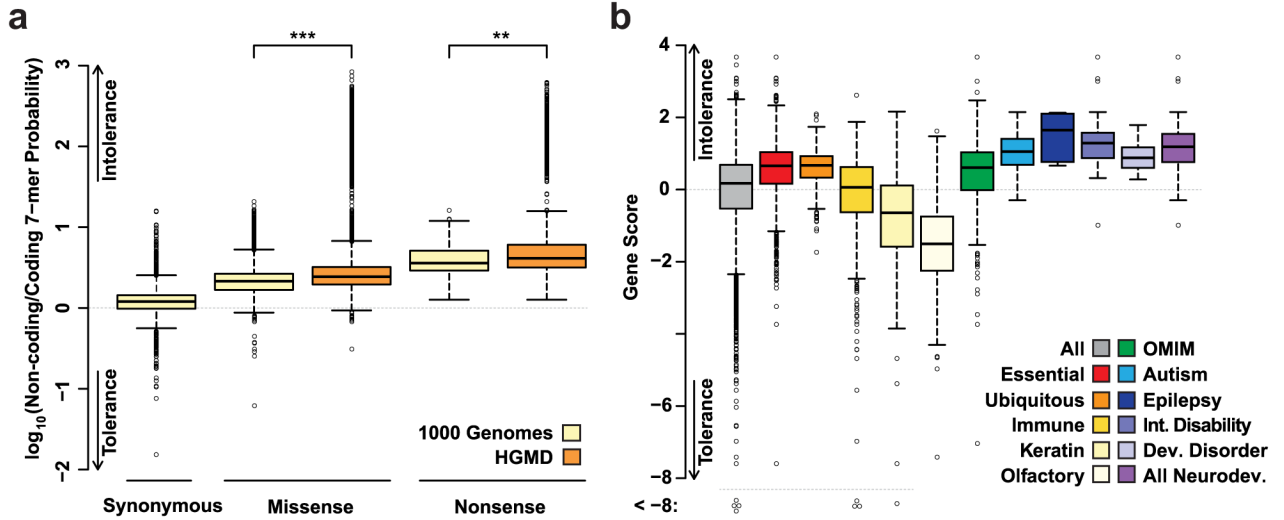


Figure 3. Prioritizing pathogenic variants and causal genes using constraint scores. **(a)** log₁₀ ratios of substitution probabilities from the 7-mer sequence context model using coding sequences matched to the intergenic noncoding sequences, for each type of substitution (synonymous, missense and nonsense) for all variants in the 1KG project or Human Gene Mutation Database (HGMD). Larger values indicate fewer substitutions in the coding genome than expected from matched noncoding sequences, consistent with the action of selective constraint. *** represents $P \ll 10^{-100}$ and ** represents $P < 10^{-29}$. **(b)** Box and whisker plot of gene scores from the model, stratified into statistically significant gene classes. Positive gene scores indicate intolerance to substitutions that change an amino acid. For the boxplot, the center line in each box denotes the median. The inter-quartile range (25th and 75th) is indicated by the ends of each box. The whiskers extend 1.5x the inter-quartile range, and data points beyond this range are plotted as open circles.

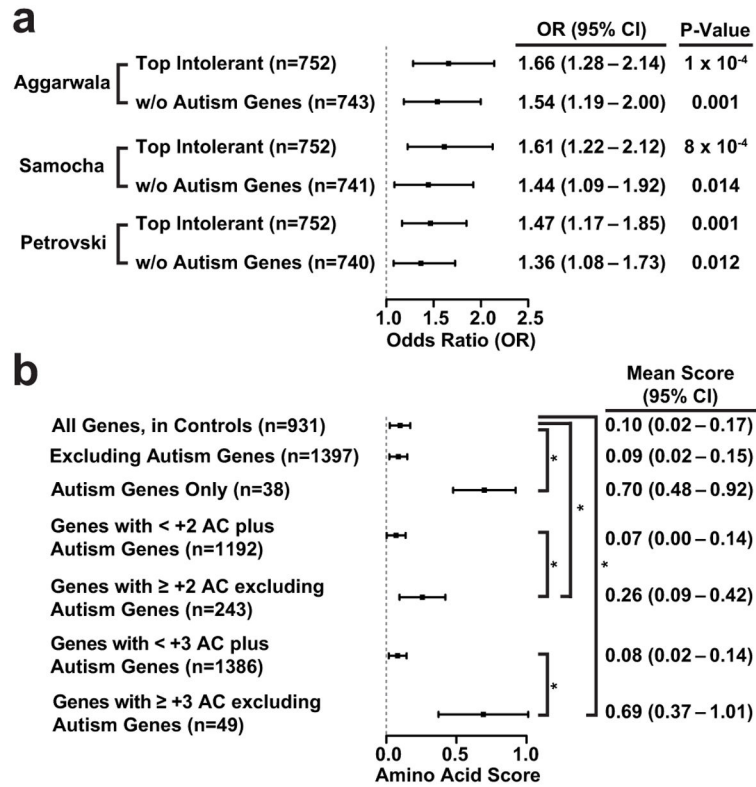


Figure 4.

Applications of gene and amino acid intolerance scores on *de novo* ASD mutational data. **(a)** Forest plot of the odds ratios (ORs), 95% confidence intervals (CIs), and p-values when comparing the *de novo* mutational burden in cases versus controls, on intolerant genes using different gene scoring methods. Scores are calculated including and excluding known Autism genes, as indicated. “Aggarwala” indicates gene scores from this report, while “Samocha” and “Petrovski” refers to the intolerant gene list from those works^{12,32}. **(b)** Forest plots of the mean amino acid scores (with 95% CIs) found from *de novo* mutations in various gene collections. Average scores were based on variants ascertained in cases, except where noted (*i.e.*, the first row: all genes in controls). W/o: without. +AC: excess count of missense or nonsense changes in cases relative to controls. For example, +3 indicates that a gene has 3 more missense or nonsense changes in cases relative to controls. *: P < 0.01.

Table 1

Summary and performance of forward regression model for feature selection using the 7-mer context in the intergenic noncoding genome. % Substitutions represents the percentage of substitutions for that class observed in the genome. # Parameters represents the number of features selected in the best 7-mer model. Model R² (7-mer) reflects prediction accuracy in the test dataset alone (not used for model training) with the best model using heptanucleotide sequence context features. Model R² (3-mer) denotes the prediction accuracy with only trinucleotide sequence context features.

| Substitution Class | # Contexts | % Substitutions | # Parameters | Model R ² (7-mer) | Model R ² (3-mer) |
|---|------------|-----------------|--------------|------------------------------|------------------------------|
| Outside CpG Dinucleotide Context | | | | | |
| A-to-C | 4,096 | 7.3 | 266 | 56.5 | 11.2 |
| A-to-G | 4,096 | 28.2 | 366 | 91.5 | 40.9 |
| A-to-T | 4,096 | 7.1 | 197 | 58.7 | 37.4 |
| C-to-A | 3,072 | 8.5 | 282 | 83.5 | 30.0 |
| C-to-G | 3,072 | 7.5 | 268 | 81.0 | 17.1 |
| C-to-T | 3,072 | 24.4 | 254 | 86.8 | 37.6 |
| Within CpG Dinucleotide Context | | | | | |
| C to A | 1,024 | 1.0 | 26 | 58.3 | 19.0 |
| C to G | 1,024 | 0.8 | 95 | 48.7 | 9.5 |
| C to T | 1,024 | 15.2 | 96 | 93.1 | 44.4 |

Enrichment of motifs identified in posterior nucleotide substitution probabilities for the 7-mer sequence context models inferred from intergenic noncoding genome. CpG+ indicates the distribution of sequence contexts which include a CpG site (4th position polymorphic site is C, 5th position fixed as G). Enrichment P-value is based on the enrichment of the motif in the 1% tail of the given substitution class: “Higher” implies enrichment in the upper 1% tail of the sequence context probability distribution, “Lower” implies enrichment in the lower 1% tail. Odds ratio and [95% CI] denotes the odds ratio (and 95% confidence interval) of enrichment of motif in the upper or lower 1% tail of the sequence context probability distribution. Fold change in substitution rate denotes the fold increase or decrease in substitution rates for the motif relative to its substitution class.

Table 2

| Motif | Substitution Class | Effect on Substitution Probability | Enrichment P-value | Odds ratio and [95% CI] | Fold change in substitution rate |
|--|--------------------|------------------------------------|---------------------|-------------------------|----------------------------------|
| NNNCGNN | C-to-T | Higher | 2×10^{-26} | 134.4 [18.4–977.4] | 13.9 |
| | C-to-G | Higher | 1×10^{-13} | 12.8 [5.9–27.7] | 2.4 |
| | C-to-A | Higher | 9×10^{-22} | 60.8 [14.6–252.1] | 2.7 |
| N[A/C/G][C/G/T]CGCG | C-to-T (CpG+) | Lower | 7×10^{-16} | 366.3 [45.6–2,939.5] | 1.5 |
| | A-to-T | Higher | 9×10^{-5} | 304.2 [31.0–2,987.6] | 12.7 |
| Poly T and Poly A combination (AAAAATTT, TTTAAAAA) | A-to-G | Lower | 5×10^{-10} | 10.2 [7.3–14.1] | 1.9 |
| Quad A (AAAAANN, NAAAAAN, NAAAAAN, NAAAAAN) | C-to-T (CpG+) | Higher | 1×10^{-10} | 102.5 [27.4–383.2] | 1.7 |
| | A-to-C | Lower | 3×10^{-4} | 9.4 [3.6–24.8] | 1.5 |
| NNTACGN | A-to-T | Higher | 2×10^{-17} | 22.3 [8.7–57.1] | 1.6 |
| | A-to-G | Higher | 1×10^{-25} | 131.2 [18.0–954.2] | 2.0 |
| NNNATNN | A-to-G | Higher | 8×10^{-53} | 5966 [2,091–17,021] | 5.1 |
| | A-to-C | Higher | | | |
| [C/T]CAAT[C/G/T]N | A-to-G | Higher | | | |